Invited paper presented at the First Int. Symp. on Diamond and Diamond-like Films, The Electrochemical Society, May 7-12, 1989, Los Angeles, CA, Paper No. 115

TRIBOLOGICAL BEHAVIOR OF CVD DIAMOND FILMS

M. N. Gardos
Hughes Aircraft Company, El Segundo, CA 90245
and
K. V. Ravi
Crystallume, Menlo Park, CA 94025

ABSTRACT

Essentially pure and sp^2-bonding contaminated, 0.8 μm thick, polycrystalline diamond films deposited on Si(100) flats were friction and wear tested against bare and pure, 40 μm thick diamond-coated α-SiC pins. The oscillatory sliding tests were performed by employing a Knudsen cell-type, wide temperature range tribometer built into a VCR-equipped, scanning electron microscope (SEM). Experiments were completed in low (10^{-5} torr) and high (10^{-1} torr) P_{air} test environments, at test flat temperatures cycled up to 850°C and back to room temperature (R.T.). The data indicate that the coefficient of kinetic friction (f_k) of diamond against itself, α-SiC and the silicon substrate is controlled by moisture and hydrogen desorption-resorption and diamond oxidation effects characteristic to certain temperature regimes and atmospheric environments. The less pure diamond film tended to delaminate from Si(100) with greater ease and wore more than its purer counterpart. The lower purity diamond layer also caused higher wear of the mating α-SiC pin due to increased generation and entrapment of fine, diamond wear debris between the frictional surfaces.

INTRODUCTION

The current surge of interest in chemical-vapor-deposited (CVD) polycrystalline diamond films is only second to that of high T_c superconducting oxides. Recent publications ranging from popular science articles, trade publications and technical papers (1 through 8) to a soon-to-be released NMAB report (9) deservingly tout the promising aspects of CVD diamond films for optical, electronic and tribological applications. While optical and electronic evaluation of the variously grown films has received considerable attention, friction and wear testing of diamond to date has been confined to single crystals (e.g., see 10, 11, 12), metal or ceramic-bonded, sintered diamond composites (13, 14), and diamond-like-carbon (DLC) coatings (15 through 20). To fill the gap in the evaluation scheme, a currently ongoing program dealing with the tribological fundamentals of solid lubricated ceramics is now determining the friction and wear properties of polycrystalline, CVD diamond films on selected ceramic substrates, for wide environmental regime applications (21 through 24). This paper represents the first comprehensive summary of the initial phases of that effort.

DIAMOND FILM DEPOSITION

Thin, 0.8 μm films of polycrystalline diamond were deposited on ~10 cm (4 in.) dia. Si(100) wafers by a DC-plasma-assisted CVD (DC-PACVD) method described elsewhere (25 through 29); for a schematic of the deposition chamber, see Fig. 1. The films were grown in 0.3% and 0.5% methane-containing hydrogen atmospheres. The processes produced essentially pure (designated hereafter a "sp^3") and sp^2-bonding contaminated ("sp^2 + sp^3") layers respectively, as analyzed by Raman spectroscopy. The wafers were photomicrographically mapped as to diamond surface morphology (i.e., highly faceted vs. cauliflowered) and diced into 7 mm x 5 mm triboflats. Two flats of the "sp^3" and one of the "sp^2 + sp^3" films were selected for friction and wear testing, making sure that the respective surface morphologies were as similar as possible (Fig. 2). SEM examination at even higher magnifications showed, however, a change of crystallite orientation within the macroscopically similar, cauliflowered structure. A predominance of a {111} surface orientation changing to a {100} orientation occurred with the increase of CH_4/H_2 ratio (i.e., there were hotter plasma conditions at the 0.5% CH_4 content). The presence of hotter plasma was corroborated by isolated droplets of the Mo counter electrode splattered on the "sp^2 + sp^3" films, as shown in Fig. 2. Similar differences in crystal orientation as a function of CH_4 content were also observed in (8). The nucleation and coalescence of diamond crystallites into a complete film on Si(100) and, consequently, the adhesion of the films was enhanced by purposely deposited, interfacial layers of DLC (25). At the boundary between the DLC and the Si surface, a SiC-like layer was observed (22). It has been shown elsewhere that a thin (~5 nm) β-SiC interface layer tends to develop at a Si/diamond junction (8).

TEST EQUIPMENT AND PROCEDURE

A controlled environment, friction and wear test stage was constructed to fit a Cambridge Stereoscan 250 Mk.3 SEM (Fig. 3). Essentially, the apparatus contains an oscillating, 7 mm x 5 mm flat sliding against a 10 mm long, 2 mm dia., hemispherically tipped pin under load. This specimen combination is housed in a differentially pumped and pressurized, Knudsen-cell-like subchamber affixed to the x-y SEM stage. The developing wear scar on the flat can be imaged, in real time, with or without a hermetically sealed lid covering the cell. With the lid on, the scar is imaged through the small (~0.5 mm dia.) Knudsen orifice drilled into the part of the lid positioned immediately above the specimen combination. The moving flat may be tested several times with the same pin, by generating parallel wear scars. These scars can be observed during tests on a TV screen and by videotaping at magnifications up to 200X. A wear path may be imaged in real time at subchamber partial pressures not exceeding 13.3 Pa = 1 x 10^{-1} torr, or in the typical atmosphere (1.33 x 10^{-3} Pa = 1 x 10^{-5} torr) of the lidless subchamber fully exposed to the turbomolecular-pumped SEM column. The thermally isolated flat can be resistively heated to 1000°C

in vacuum or in various, selected gas atmospheres. Further details on apparatus construction and typical performance may be found in (22). This SEM tribometer has been used to measure the surface shear strength (and in some cases, the critical resolved shear stress) of single crystal CaF_2 and BaF_2 (22) and oxygen-deficient Magnèli phases formed in single crystal rutile (TiO_{2-x}), see (30).

In the present case, the flats diced from the diamond-coated Si wafers were oscillated against the bare or diamond coated α-SiC pins under a 0.49 N load, at an average velocity of 4.7×10^{-3} m•sec^{-1}. The schematic of three types of test combinations is given in Fig. 4. The triboflat edge sites showing columnar crystal morphologies and thickness of diamond films, as well as the size of the α-SiC pin tip wear scars corresponding to these new flats are depicted in Fig. 5. All specimens were repeatedly cleaned before tests in boiling, spectroquality-grade hexane, followed by drying in air.

The test procedure with each test combination basically consisted of sliding first in 10^{-5} and then in 10^{-1} torr at room temperature to observe the effects of desorbing atmospheric contaminants and an increased presence of oxygen. This brief, initial period was then followed by heating a flat to ~850°C, then cooling it back to room temperature; f_k was measured continuously during sliding, as a function of temperature and the number of cycles. The rate of heating and atmospheric cycling was intentionally not standardized from test-to-test to help clarify either time (number of cycles) or temperature dependence of friction phenomena. Each flat received several tests under various atmospheric conditions by repeatedly reusing the mating pin (Fig. 6).

The used flats and the worn α-SiC pin tips were examined photomicrographically in the SEM and under an optical microscope. The chart-recorded data were reduced by digitizing and logging the coefficients of friction (f_k) versus the number of cycles, atmosphere and temperature of a given test, because direct digitizing into a computer was not yet available. The data were then analyzed by data logging and analysis software running on a high-capacity, desk-top computer connected to a plotter.

DATA AND DISCUSSION

Friction of Base α-SiC vs. Diamond-on-Silicon

The f_k values (also designated as COF) of α-SiC vs. "sp^3" sliding in 10^{-5} torr are shown in Fig. 7a and 7b. The 10^{-1} torr test results are given in 7c, representing Run No. 4 in Fig. 6a. The data from Run No. 3 are not presented, because the diamond film seemed to begin delamination there at R.T., after only a few hundred cycles. Higher magnification SEM examination did not show that the frictional

variations normally associated with film peeling were caused by gross delamination.

The COF of the two α-SiC vs. "sp^2 + sp^3" 10^{-5} torr tests are enclosed in Fig. 8a and 8b; the 10^{-1} torr test is represented by Fig. 8c, all corresponding to the three wear paths shown in Fig. 6b.

Both the pure and the sp^2-contaminated coatings displayed essentially the same friction behavior during R.T. sliding. The lowest f_k always developed after some sliding at, or near, room temperature (R.T.). This reduction in friction from ~0.5+ to as low as 0.06 in 10^{-5} torr is attributed to the desorption of atmospheric contaminant gases from the diamond surface, mainly moisture. Although our SEM tribometer has no in-situ surface analytical capability, other recent analyses of pulverized and single-crystal diamond, as well as the same polycrystalline CVD films used here (31) indicated that oxygen (not hydrogen) is the most predominant species on the diamond surface. As Goddard discussed it in (32), the surface of unpolished diamond is unstable and is easily oxidized due to the presence of dangling bonds. Polishing with a diamond-hydrocarbon slurry caps the dangling bonds with hydrogen, also see (33). Although one would expect a CVD diamond film surface to be saturated with hydrogen, it is known that great experimental care must be exercised to prevent oxygen contamination of the diamond surface during hydrogenation (33). Our DC-PACVD chamber plumbing was air-tight, but was not checked against ultrahigh vacuum technology standards. Some slight oxygen (air) contamination of the process gases was possible. It should not be surprising, therefore, that oxidation-hydration of the diamond film surface can occur during the final phases of growth or just by extended storage in air afterwards. Dry polishing (111) diamond also leaves the surface contaminated with oxygen (33). Grinding of graphite into powder in various media represents a parallel example. Grinding under hexane produces oleophilic surfaces, while grinding in air results in surfaces which are hydrophilic (34).

Lending credence to our friction data and hypothesis are the results of Enke and coworkers (15, 16): in friction tests of DLC layers, the f_k in 10^{-8} torr P_{H_2O} was 0.01 - 0.02, but above 10^{-1} torr P_{H_2O} f_k rose to 0.19 at 100% relative humidity. According to Orzeszko et al (35), moisture resides mainly on the surface of DLC. In cases where there is some apparent penetration ($\leq$5 nm), they postulated that the water simply fills the void regions of a "rough" surface. It is noteworthy that a heat lamp could not remove all the water.

The mechanism of adsorption goes beyond a simple, capillary-fill phenomenon. First and foremost, it is more likely that the surface-oxidized diamond or DLC layer sorbs moisture by hydrogen bonding. Similarly, the oxidation products of graphite are CO and CO_2 (gases) and graphite oxide (a solid), see (36). This solid demonstrates high stability at normal temperatures because of its covalency. No definite stoichiometry can be assigned to it; however, an idealized formula of

$C_8O_2(OH)_2$ has been postulated. Unfortunately, no equivalent data on "diamond-oxide-hydroxide" formation and analyses could be found beyond what exist in (31 through 33). Interestingly, sliding in 10^{-1} torr, at R.T., never resulted in f_k as low as observed in 10^{-5} torr, regardless of diamond purity.

Purity notwithstanding again, heating diamond to 800°C+ is invariably accompanied by a substantial increase in friction. Our results essentially confirm those of Pepper (38), who showed that the appearance of unoccupied states in the band gap (i.e., dangling bonds) on heated diamond surfaces was accompanied by drastically increased friction of a diamond-metal couple. Subsequent hydrogen saturation of the surfaces reduced the friction due to annihilation of dangling bonds by capping with hydrogen. Our friction data are especially interesting from three standpoints: (1) there seem to be two major hydrogen desorption and resorption regions, one at ~400°C, the other at 600° to 850°C, see Fig. 7b, (2) the desorption-resorption-induced friction effects occurred even though some sliding-induced transfer of the α-SiC to diamond did occur, and (3) the friction at ~850°C is always substantially lower in 10^{-1} torr than in 10^{-5} torr. We suspect that the gas removal regions may coincide with the desorption of H_2 at ~400°C and atomic hydrogen in the higher temperature regime, similar to what happens during sliding diamond against silicon (see forthcoming discussion). Landstrass and Ravi (29) did show that hydrogen begins to leave the diamond film at temperatures as low as 100°C, as evidenced by electrical resistivity changes. On transferring an α-SiC (partial) film to diamond (Fig. 9) one may argue that a similar increase in f_k of a heated α-SiC vs. metal couple [attributed to a variety of causes, but not specifically to dangling bond generation, see (12, 37)] is what we actually observed. As shown in these papers, at and beyond 850°C f_k decreased drastically due to graphitization of the α-SiC surface. We agree that at higher P_{air}, the oxidation-graphitization of the diamond and α-SiC surfaces at ~850°C could generate a sufficient "third body" interfacial layer to achieve reduction in f_k. Yet, cooling to R.T., see Fig. 7c, (or just suddenly reducing P_{air} at 850°C, see Fig. 8c) immediately restitutes higher friction at least momentarily, before the hydrogen resorption-induced reduction in f_k manifests itself. This f_k spike can happen only if the "third body" was no longer formed in sufficient quantities and is removed by rubbing, temporarily allowing the generation of dangling bonds. On further cooling and sliding, hydrogen resorption from the relatively low grade vacuum of the SEM column could (and did) bring f_k down.

The remarkable similarities in all of the corresponding friction data discount any major influence of the smeared or oxidized Mo droplets on the "$sp^2 + sp^3$" surface.

Wear of Bare α-SiC vs. Diamond-on-Silicon

The average, sliding-distance-normalized wear rates of each of the two α-SiC pins repeatedly rubbed against their respective "sp^3" or

"sp^2 + sp^3" flats are presented in Table 1. These rates are specific to our test procedures (low-high temperatures, sliding in 10^{-5} and 10^{-1} torr, various heating rates, reused pins, etc.). Furthermore, our wear rates were calculated based on a spherical segment volume loss, itself determined by the α-SiC pin wear scar sizes depicted in Fig. 5. These rates are only rough averages of all tests of a given set, because the pin wear scar size (therefore the unit load) changes rapidly in a sphere-on-plane sliding configuration (38). Nevertheless, as indicated by the enclosed data from (14), the approximate α-SiC wear rates are close to that reported by Mehan et al against a somewhat softer, less abrasive composite of diamond particles embedded in a Si + SiC matrix.

From the tribological standpoint, thin solid lubricant films can fail in two ways: (1) they delaminate prior to wear-through due to poor interfacial adhesion at the transmitted interfacial stresses or, (2) they wear through gradually (fast or slow) without sudden delamination. Since the interfacial stresses depend on coating and substrate modulus and Poisson's ratio, coating surface shear strength and thickness, load and real area of contact, intra/interfilm stresses, etc. in a complex manner (39, 40), a coating can wear gradually before delaminating, or it can delaminate almost instantly.

The photomicrograph in Fig. 6a shows that the "sp^3" film partially delaminated during the first 10^{-5} torr test. The video-log indicated that delamination began at ~825 cycles, where f_k increased to 0.7+ due to heating. Gross delamination was initiated at the ends of the strokes, where the break-away (static) friction peak was always higher that the peaks of the kinetic friction coefficient (f_k). The dumb-bell-like delamination pattern shown in Fig. 6a (Run No. 1) developed rapidly between 850 and 1000 cycles, at which time the test was terminated. Note that (a) during Run No. 1 the unit loads were the highest because we started testing with a new pin and, in spite of the high loads, (b) even at the end of the test, the middle of the wear path did not seem to delaminate enough to allow complete contact of the worn pin tip with the silicon substrate (i.e., some part of the pin was always sliding on some diamond). Due to large differences in surface charging (the less conductive "sp^3" always charged more than the more conductive "sp^2 + sp^3," and the most conductive Si(100) doped with boron charged the least), the degree of delamination pattern and its development was clearly visible in the SEM.

The black, mottled appearance of the other three wear tracks in Fig. 6a was not always caused by the kind of α-SiC transfer depicted in Fig. 9. On small spots of this "sp^3" film, where charging differences of the rubbed film indicated more sp^2-bonding than other areas, occasional delamination of the film did occur on the microscale basis. The surrounding, highly charged (i.e., purer) areas did not delaminate, however.

The observation that the "sp^2 + sp^3" film is not bonded to the substrate as well as the "sp^3" homolog was somewhat confirmed by the

tests in Fig. 6b. We speculate that the only reason Run No. 1 did not delaminate in a gross fashion even after ~1000 cycles (also see Fig. 8a) is because the greater wear of the "sp^2 + sp^3" film provided a wider wear scar (i.e., lower unit loads) fast. As shown in Fig. 6b, however, the onset of peeling can be seen at the very ends of the stroke and at the edge of the wear tracks. Even under a worn pin, Run No. 2 delaminated at ~325 cycles (see Fig. 8b), just as heating began to increase the friction. Run No. 3 (10^{-1} torr) did not delaminate, although high magnification photomicrographs of the very wide wear track (sliding against the most worn pin providing the lowest unit loads) indicated incipient coating failure everywhere in the track.

The photomicrographs in Fig. 6a and 6b (and others at higher magnifications not shown here) indicate a great deal more wear debris at the ends of the strokes of the "sp^2 + sp^3" than on the "sp^3" layer. The main reason for the higher wear of the sp^2-contaminated films may be deduced from Fig. 10 and 11. Regardless of the atmosphere, the pure "sp^3" wears as originally hypothesized by Crompton et al (41) and now commonly accepted by others (42): diamond wear is caused by small diamond fragments (10 to 100 nm in dimensions) dislodged from the diamond surface by rubbing, indentation or impact. In the diamond trade, "soft" or "easy" polishing directions on a single crystal are "determined mainly by the ease with which microscopic octahedral-faced fragments can be pulled out of the surface being polished." Less debris formed is commensurate with a lesser amount of "third body" diamond debris reservoir between the sliding surfaces. In Fig. 10, the wear surface of "sp^3" remains facetted, even while in the incipient failure mode. Next to the exposed, flat Si(100)/DLC substrate (somewhat charging), the diamond crystallites of the worn film (highly charging) consist of submicron-size facets of still-fused crystallites strongly anchored to the DLC interface film at the nucleation sites. There appears to be little loose debris on top.

The worn surface of the "sp^2 + sp^3" layer is radically different (Fig. 11). At the edge of the path worn into the Si(100) substrate, the surface of the residual diamond film is not facetted, but appears highly polished. It also exhibits a marbled appearance, as if the non-charging columnar growth boundaries of the cauliflowered films (43) were more conductive (perhaps more sp^2-bonding-contaminated) than the bulk of the columns. The polished appearance of the "sp^2 + sp^3," combined with this observation indicate a composite-like nature of the more sp^2-contaminated films grown at higher CH_4 contents, as speculated by Nemanich et al (44, 45). According to their hypothesis, the grain boundaries always contain more sp^2-contaminated (i.e., weaker and softer) diamond. As such, an "sp^2 + sp^3" layer resembles certain hot-pressed Si_3N_4, and Co-WC cermets or other bonded (sintered) hard-grain materials, where the grain boundaries are always the weak links in the structural integrity of the monolithic composites. This has been further confirmed by the observation that grain boundaries in diamond films oxidize at a significantly higher rate than the diamond grains (46).

The microfragmentation of "$sp^2 + sp^3$" is therefore enhanced, resulting in greater wear. The microfragments are small enough to leave a highly polished surface behind. The larger number of microfragments become entrapped between the sliding surfaces, however. This, in turn, causes greater wear of the α-SiC counterface also, as depicted in Fig. 5 and shown more quantitatively in Table 1.

Friction and Wear of Diamond-on-SiC vs. Diamond-on-Si(100)

The highly facetted, but still cauliflowered, ~40 μm "sp^3" on the α-SiC pin repeatedly and almost immediately removed the much thinner (0.8 μm) "sp^3" from the Si flat during the 10^{-5} torr test. The video-log indicated the onset of film delamination as early as after 200 cycles, with complete peeling and removal of all diamond film at ~600 cycles, as indicated in Fig. 12. Since the 10^{-1} torr test also suffered early delamination in ~200 cycles, f_k data against oxidized silicon surfaces is not presented here.

Up to the point of delamination, the f_k trend of "sp^3" vs. "sp^3" is the same as the α-SiC vs. "sp^3" or "$sp^2 + sp^3$." The initial friction is high, and after some sliding it drops to a lower value characteristic to the sliding combination. Here, this value is ~0.20. It is most significant that complete delamination occurred where the friction rose precipitously from ~0.25 to 0.5, at ~350°C. It is known that at 350° to 375°C some silicon-hydrogen bonds are broken in either amorphous (47, 48) or crystalline (49, 50) Si, by thermal agitation. In that temperature range, hydrogen from SiH_2 species is desorbed to create double Si dangling bond defect sites (Si<), whereas hydrogen from the SiH species is desorbed around 600° to 800°C (48, 49) to form single (Si-) defect sites. The reactivity and amorphization of a crystalline Si surface is enhanced by the production of active sites either by ion bombardment (51) or by lapping (as Si wafers normally polished), see (52). This enhanced reactivity affects friction and the ability to keep hydrogen on the surface simultaneously. It makes sense, therefore, that any reconstruction of the Si surface that may have followed H_2 desorption at ~350°C (self-annihilating the dangling bonds and thereby reducing friction) is followed by a large f_k peak at 850°C. Why? Single Si- dangling bonds are generated there on desorption of atomic hydrogen from a triboactivated surface.

Similar to what happens to the CH_2 and CH species' hydrogen desorption and resorption off-on diamond on heating and cooling, hydrogen from the vacuum chamber atmosphere passivates the Si surface by occupation of the Si dangling bonds. We speculate that another Si surface reconstruction and dangling bond rearrangement on cool-down, at near R.T., is suspected. There, f_k temporarily rose again to ~0.5, followed by a reduction to ~0.1 at 1800 cycles. This last friction peak may signify first a temporary generation, followed rapidly by capping of Si< dangling bonds on further cool-down to R.T. Along these lines, similar passivation of Si surfaces with hydrogen and

hydrocarbons has been reported in the literature, as also discussed in (51, 52, 53).

The examination of Fig. 5c indicates a very small amount of diamond removed from the tip of the coated α-SiC pin. After all, most of the sliding occurred not against diamond, but bare silicon. As a result (see Table 2), the wear rate of "sp^3" vs. "sp^3" and eventually bare silicon is significantly less than that of α-SiC vs. diamond in Table 1. Nevertheless, this very low wear rate scales well with other available literature data on similar combinations.

Actually, the ~6 x 10^{-17} $m^3/N \cdot m$ rate is presumed to be higher than actual, because the wear scar on the diamond-covered pin tip is not a perfect circle. It can be seen at the higher SEM magnification in Fig. 13 that the scar consist of a collection of flat plateaus formed only on the tips of the cauliflowered diamond morphology. It follows, therefore, that the initial unit loads were much higher than the ≅6.9 GPa based strictly on Hertzian stress calculations of a diamond vs. diamond sphere-on-plane contact. According to Crompton et al (41), at such enormous unit loads f_k values as low as 0.1 can generate enough surface shear to induce tensile cracks on the diamond surface (Fig. 14). The facts that (a) the data show high friction (f_k = 0.6 to 0.7) at the onset of the tribotest (see Fig. 12), and (b) similarly high values of friction were reached no less than three more times during the test, the development of diamond tensile cracks aligned mostly normal to the direction of sliding was inevitable (Fig. 13).

These data not only give insight to the polishing mechanism of diamond, but indicate a means for accelerated or decelerated testing of diamond wear by controlling the coefficient of friction. In the present case, control is by extrinsic (i.e., environmental) influences. Future work needs to involve alteration of the diamond surface by intrinsic (i.e., molecular-engineering-induced) means, such as full hydrogenation by polishing with a hydrocarbon oil-diamond paste, prefluorination of the diamond surface or lubrication of diamond with other, thin fluid or solid films.

CONCLUSIONS

For the first time, controlled-environment friction and wear testing of essentially pure and sp^2-bonding contaminated, polycrystalline CVD diamond films were completed using a specially designed, wide temperature range tribometer. In the absence of in-situ surface analytical capability, the friction and wear data were combined with information from the literature to demonstrate that the friction of the films is highly dependent on the surface chemistry of the films. Surfaces capped with adsorbates such as oxygen and moisture yield high (0.5 to 0.8) friction, and those saturated with hydrogen yield low (~0.1) friction. These findings appear to be valid for α-SiC vs.

diamond, diamond vs. silicon and, to some degree, diamond vs. diamond sliding combinations.

The wear of CVD diamond layers seems to depend on the degree of sp^2 contamination. A more contaminated film tended to delaminate from the Si(100) substrate and wear more against α-SiC than the purer version. Higher wear may be attributed to the composite-like nature of the "sp^2 + sp^3" diamond, in that the grain and columnar growth boundaries within the film are the most contaminated and, at the same time, are the weakest. The less pure diamond film also caused higher wear of the mating α-SiC counterface due to increased self-generation of fine wear debris (i.e., a polishing medium) trapped between the frictional surfaces. Enhanced tensile cracking of the diamond surface under high friction conditions and high loads appears to be the initiating step of the diamond film's wear mechanism, under tangential shear conditions.

It is hoped that other, currently ongoing tribotests combined with in-situ surface analytical capabilities, performed on identical diamond films deposited on single crystal silicon in various test atmospheres (54), will soon confirm or modify the hypotheses presented in this paper.

ACKNOWLEDGEMENTS

The authors are greatly indebted to L. Plano, S. Yokota and J. M. Pinneo of Crystallume for growing the diamond films and B. L. Soriano, P. S. Davis, G. L. Meldrum and B. Buller of Hughes Aircraft Company for performing the tribotests and reducing the data. The help of J. E. Butler of the Naval Research Laboratory is also gratefully acknowledged for surface analytical examination of the diamond films. This research was completed under the auspices of the DARPA/Hughes "Determination of Tribological Fundamentals of Solid Lubricated Ceramics" program, DARPA Order No. 5177, AFWAL Contract No. F33615-85-C-5087, with B. D. McConnell acting as the AFWAL Project Engineer. The Crystallume diamond deposition study was completed under Hughes P.O. P519308-SLX.

REFERENCES

1. G. Graff, Popular Sci., 233 (3), pp. 58-60 (1988).

2. M. Simpson, New Scientist, 117 (1603), pp. 50-53 (1988).

3. B. Manz, Microwaves & RF, 27 (5), pp. 37-45 (1988).

4. L. Connor, M. Pinneo, Photonics Spectra, 23(1), pp. 132-124 (1989).

5. R. C. DeVries, Ann. Rev. Mater. Sci., 17, pp. 161-187 (1987).

6. J. C. Angus, and C. C. Hayman, Science, 241, pp. 913-921 (1988).

7. K. Srikanth et al, Thin Solid Films, 164, pp. 187-190 (1988).

8. B. E. Williams, and J. T. Glass, J. Mater. Res., 4, pp. 373-384 (1989).

9. Diamonds and Diamond-like Materials: An Emerging Technology, Status and Applications, Report of the Committee on Superhard Materials, National Materials Advisory Board Report No. 445, National Academy Press, 1989.

10. I. P. Hayward, and J. E. Field, 50 Years of Tribology, Proc. Inst. Mech., Eng., (Lond.), Paper No. C159/87, 1987.

11. I. P. Hayward, "The Friction and Strength Properties of Diamond," Ph.D. Thesis, U. of Cambridge, U.K., 1987.

12. K. Miyoshi, and D. H. Buckley, Applications of Surf. Sci., 6, pp. 161-172 (1980).

13. R. L. Mehan, and S. C. Hayden, Wear, 74, pp. 195-212 (1981-82).

14. R. L. Mehan, C. I. Hejna, and M. D. McConnell, J. Mater. Sci., 20, pp. 1222-1236 (1985).

15. K. Enke, H. Dimigen and H. Hübsch, Appl. Phys. Lett., 36, pp. 291-292 (1980).

16. K. Enke, Thin Solid Films, 80, pp. 227-234 (1981).

17. C. Weissmantel et al, Thin Solid Films, 96, pp. 31-44 (1982).

18. J. Koskinen, J.-P. Hirvonen, and A. Antilla, Appl. Phys. Lett., 47, pp. 941-943 (1985).

19. A. Antilla et al, Appl. Phys. Lett., 50, pp. 132-134 (1987).

20. J. Koskinen, J. Appl. Phys., 63, pp. 2094-2097 (1988).

21. M. N. Gardos, Determination of Tribological Fundamentals of Solid Lubricated Ceramics, Part I: Fundamental Studies, Fourth Semiannual Report for the period 01 April 1987 to 31 October 1987, Contract No. F33615-85-C-5087, Hughes Aircraft Company, El Segundo, CA 90245, November 1987.

22. ibid, Fifth Semiannual Report, June 1988.

23. ibid, Sixth Semiannual Report, March 1989.

24. K. V. Ravi et al, Proc. 3rd SDIO/IST-ONR Diamond Tech. Initiative Symp. (Extended Abstracts and Presentation Summaries), Crystal City, VA, 12-14 July 1988, Paper No. Th6.

25. Ibid, Paper No. T21.

26. J. Narayan et al, Appl. Phys. Lett., 53, pp. 1823-1825 (1988).

27. K. V. Ravi et al, in Proc. First. Int. Conf. on New Diamond Sci. & Technol., Tokyo, Japan, Oct. 24-26, 1988.

28. K. V. Ravi and M. I. Landstrass, Proc. "High Frequency Power Conversion '89" Symp., Naples, FL, May 14-19, 1989.

29. M. I. Landstrass and K. V. Ravi, paper submitted to Appl. Phys. Lett., Apr. 1989.

30. M. N. Gardos, paper presented at the 44th STLE Annual Meeting, in Atlanta, GA, May 1-4, 1989; STLE Preprint No. 89-AM-78-1.

31. D. E. Patterson, R. H. Hauge, and J. L. Margrave, in New Materials Approaches to Tribology: Theory and Applications, Proc. MRS 1988 Fall Meeting, Symp. S, Nov. 29 - Dec. 2, 1988, Boston, MA.

32. W. A. Goddard III, Eng. & Sci. (Cal. Inst. of Tech.), XLIX (1), pp. 2-8 (1985).

33. B. B. Pate, Surf. Sci., 165, pp. 83-142 (1986).

34. A. J. Groszek, and R. E. Witheridge, ASLE Trans., 14, pp. 254-266 (1971).

35. S. Orzeszko et al, J. Appl. Phys., 64, pp. 4175-4180 (1988).

36. K. Leong, W. C. Forsman, and F. L. Vogel, Mat. Sci. Eng., 64, pp. 149-155 (1984).

37. K. Miyoshi, D. H. Buckley, and M. Srinivasan, Cer. Bull., 62, pp. 494-500 (1983).

38. K. R. Mecklenburg, ASLE Trans., 17, pp. 149-157 (1974).

39. M. N. Gardos, in New Materials Approaches to Tribology: Theory and Applications, Proc. MRS 1988 Fall Meeting, Symp. S., Nov. 29 - Dec. 2, 1988, Boston, MA.

40. M. N. Gardos, Lubr. Eng., 44, pp. 400-407 (1988).

41. D. Crompton, W. Hirst, and M. G. W. Howse, Proc. Roy. Soc. A., 333, pp. 435-454 (1973).

42. R. H. Wentorf, R. C. DeVries, and F. P. Bundy, Science, 208, pp. 873-880 (1980).

43. R. Messier and J. E. Yehoda, J. Appl. Phys., 58, pp. 3739-3746 (1985).

44. R. J. Nemanich et al, Proc. 3rd SDIO/IST-ONR Diamond Tech. Initiative Symp. (Final Program and Presentation Summaries), Crystal City, VA, 12-14 July 1988, Paper No. T.16.

45. R. J. Nemanich et al, J. Vac. Sci. Technol., A6, pp. 1783-1787 (1988).

46. L. Plano, S. Yokota and K. V. Ravi, paper presented at this Symposium, Paper No. 105.

47. J. O. Olowolafe, Thin Solid Films, 161, pp. 181-185 (1988).

48. Y. Mishima, and T. Yagishita, J. Appl. Phys., 64, pp. 3972-3974 (1988).

49. V. V. Kveder, R. Labusch, and Yu. A. Ossipyan, Phys. Stat. Sol. (A), 84, pp. 149-156 (1984).

50. P. Gupta, V. L. Colvin, and S. M. George, Phys. Rev. B, 37, pp. 8234-8243 (1988).

51. M. J. Bozack et al, J. Appl. Phys., 60, pp. 3750-3754 (1986).

52. M. Stutzman et al, Appl. Phys. Lett., 52, pp. 1667-1669 (1988).

53. J.-G. Lee, and S. R. Morrison, J. Appl. Phys., 64, pp. 6679-6683 (1988).

54. Personal communications with I.P. Hayward (Naval Research Laboratory, Wash. D. C.) and L. E. Pope (Sandia National Laboratories, Albuquerque, NM), Apr. 1989.

TABLE 1. THE WEAR OF POLYCRYSTALLINE α-SiC AGAINST POLYCRYSTALLINE DIAMOND COUNTERFACES.

Pin	Disc or Flat	Pin (α-SiC) Wear Rate ($m^3/N \cdot m$)	Reference
Sintered α-SiC	Poly-XTL Diamond Composite (Si + SiC)	1.55×10^{-15}	(14) (1)
Sinter-HIP α-SiC	0.8 μm "sp^3" Film on Si(100)	2.65×10^{-14}	Present Work (2)
Sinter-HIP α-SiC	0.8 μm "$sp^2 + sp^3$" Film on Si(100)	7.76×10^{-14}	Present Work (3)

(1) Pin-on-disc test; 4.4 to 40.1 N loads, 1.25 $m \cdot sec^{-1}$, unidirectional speed, in air.
(2) 34.2 m total sliding, see Fig. 6a.
(3) 25.6 m total sliding, see Fig. 6b.

TABLE 2. THE WEAR OF SINGLE CRYSTAL AND POLYCRYSTALLINE DIAMOND AGAINST SELECTED HARD COUNTERFACES.

Pin	Disc or Flat	Pin (Diamond) Wear Rate ($m^3/N \cdot m$)	Reference
(001) Diamond	α-SiC Abrasive Wheel	3.06×10^{-17}	(41) (1)
Poly-XTL Diamond Composite (Si + SiC)	Poly-XTL Diamond Composite (Si + SiC)	5.66×10^{-17}	(14) (2)
40 μm "sp^3" Film on Sinter-HIP α-SiC	0.8 μm "sp^3" Film on Si(100)	$\sim 6 \times 10^{-17}$	Present Work (3)

(1) Pin-on-disc test; 2N load, 8.8 $m \cdot sec^{-1}$, unidirectional speed, in air.
(2) Pin-on-disc test; 4.4 to 40.1 N loads, 1.25 $m \cdot sec^{-1}$, unidirectional speed, in air.
(3) 25.2 m total sliding, first on diamond film then, after delamination, on the exposed Si(100) substrate; see Fig. 6c.

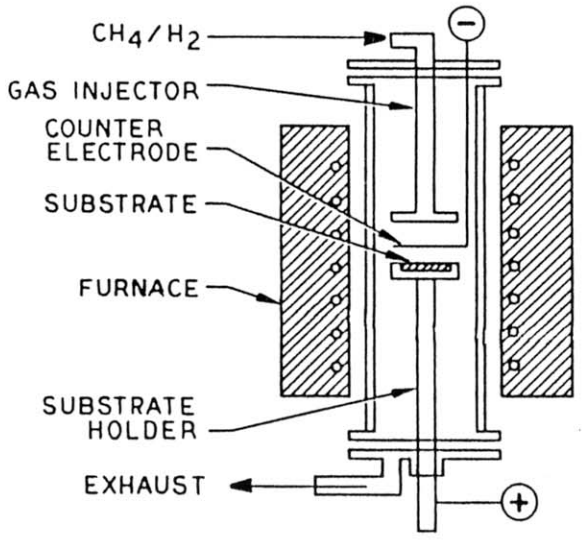

Figure 1. Schematic of DC-PACVD chamber.

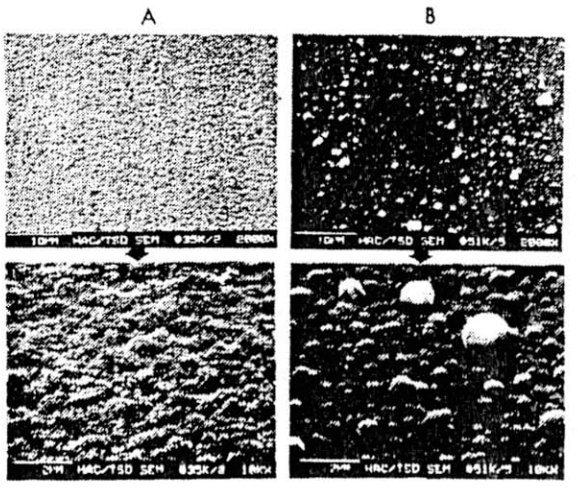

Figure 2. SEM photomicrographs of diamond film topography and structure on triboflats: (a) "sp^3" film, (b) "sp^2 + "sp^3" film (note charging droplets of the molten Mo counter electrode).

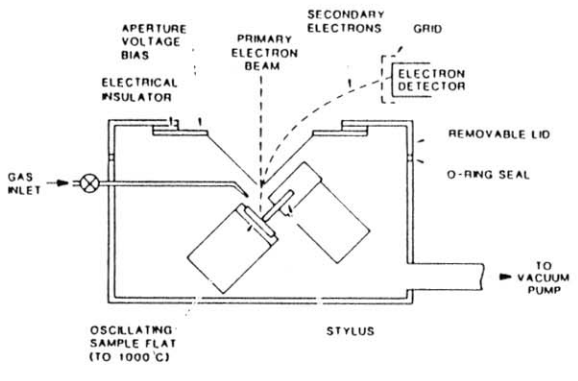

Figure 3. Schematic of SEM tribometer.

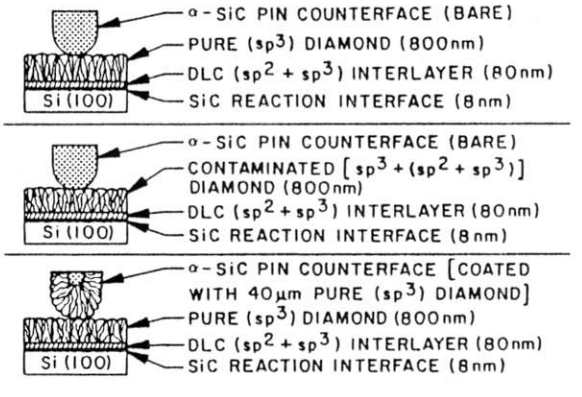

Figure 4. Schematics of test combinations.

Figure 5. SEM and optical photomicrographs of as-deposited diamond film structures on Si(100) triboflats and their mating (worn) α-SiC tribopins; (a) "sp^3" vs. α-SiC; (b) "sp^2 + sp^3" vs. α-SiC; (c) "sp^3" vs. "sp^3"; arrows next to wear scars indicate direction of sliding.

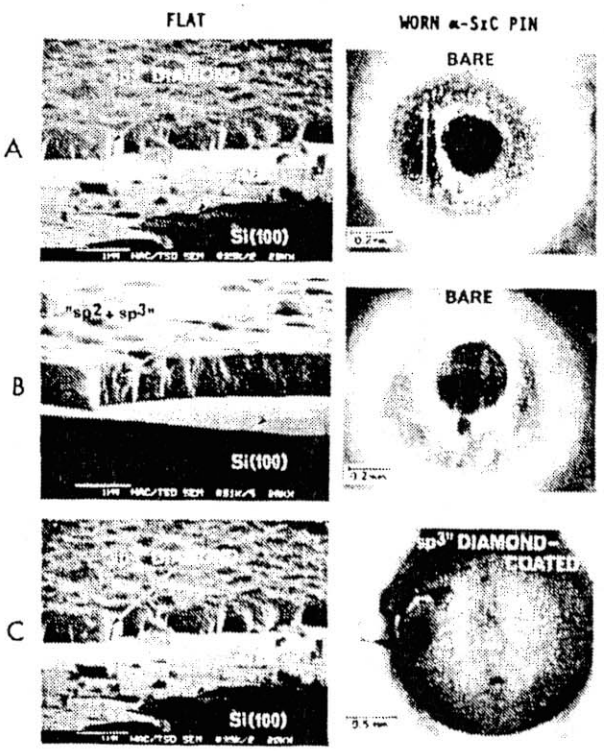

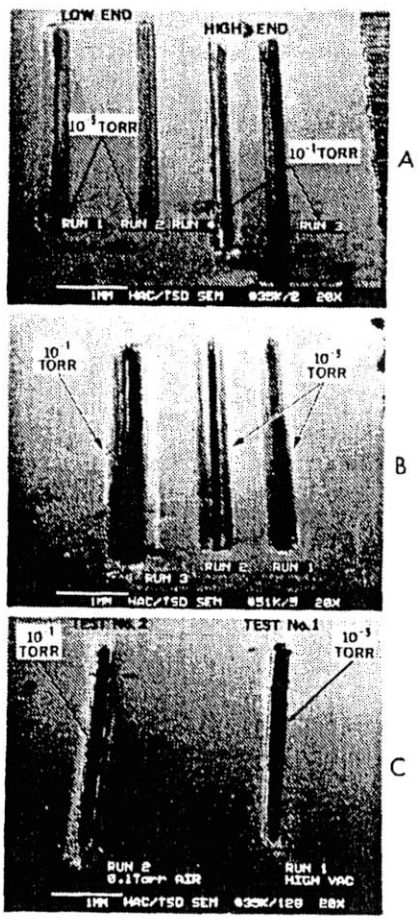

Figure 6. SEM photomicrographs of worn triboflats (a) "sp^3" vs. α-SiC, (b) "sp^2 + sp^3" vs. α-SiC, (c) "sp^3" vs. "sp^3" tests in 10^{-5} and 10^{-1} torr P_{air}, as indicated.

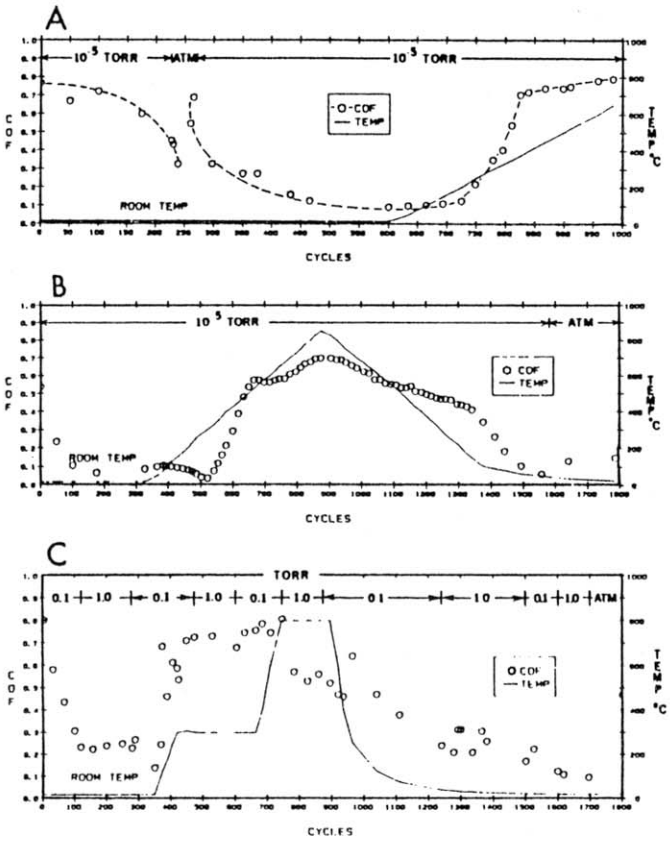

Figure 7. Coefficients of friction of "sp^3" vs. α-SiC as a function of temperature and pressure see Fig. 6a: (a) Run No. 1, (b) Run No. 2, (c) Run No. 4.

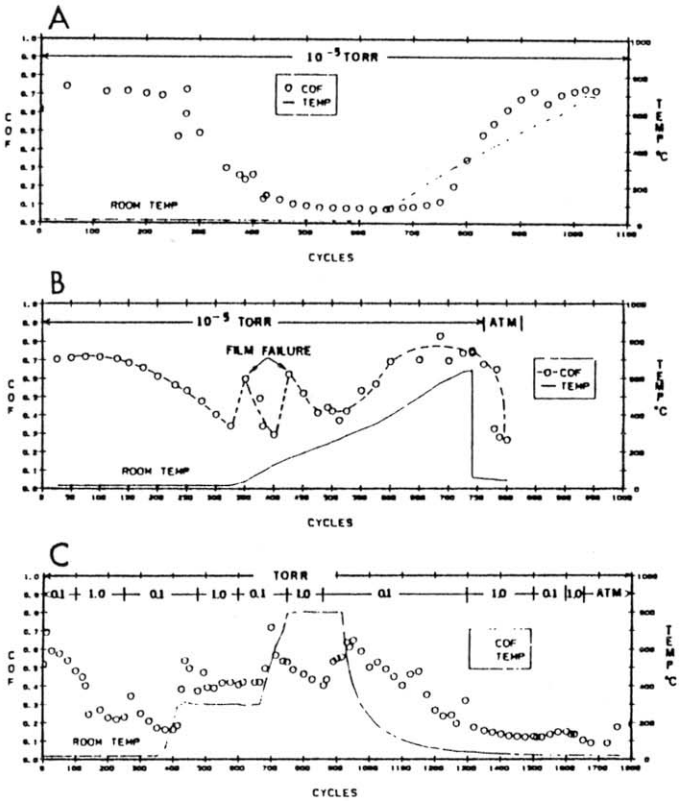

Figure 8. Coefficients of friction of "sp^2 + sp^3" vs. α-SiC as a function of temperature and pressure; see Fig. 6b: (a) Run No. 1, (b) Run No. 2, (c) Run No. 3.

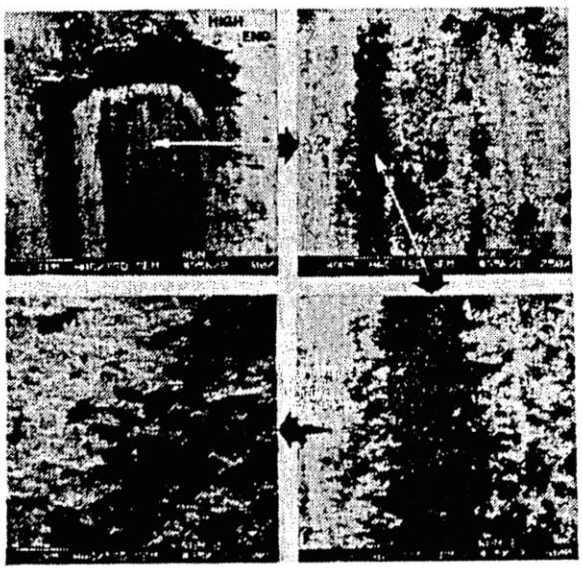

Figure 9. Transferred α-SiC film on "sp^3" diamond layer.

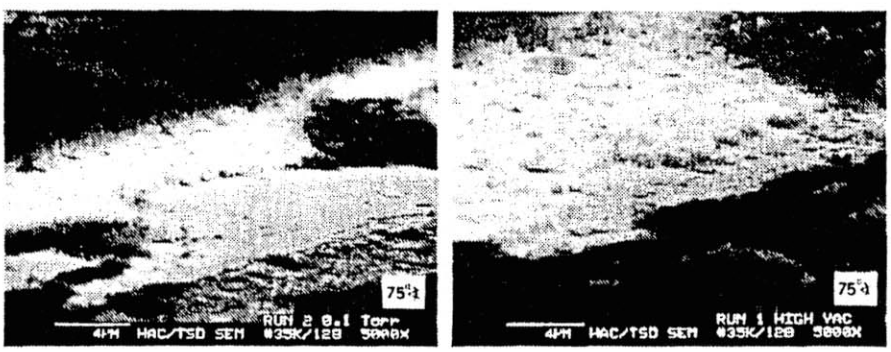

Figure 10. Low-angle SEM photomicrographs of the worn "sp^3" layer on the Si(100) substrate (edge of wear scar); in 10^{-1} torr and 10^{-5} torr.

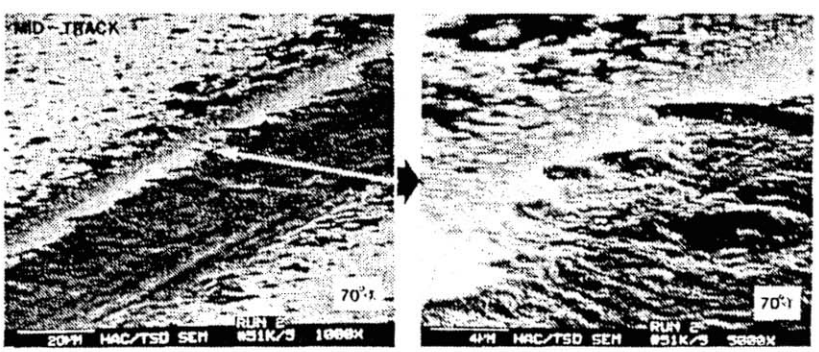

Figure 11. Low-angle SEM photomicrographs of the worn "$sp^2 + sp^3$" layer on the Si(100) substrate (edge of wear scar); in 10^{-5} torr.

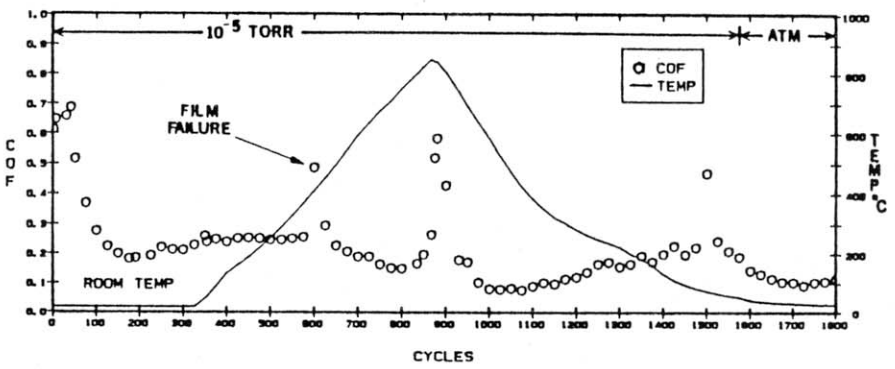

Figure 12. Coefficients of friction of "sp^3" vs. "sp^3" as a function of temperature and pressure, followed by "sp^3" vs. Si(100) substrate interaction after diamond film delamination; see Fig. 6c, Run No. 1.

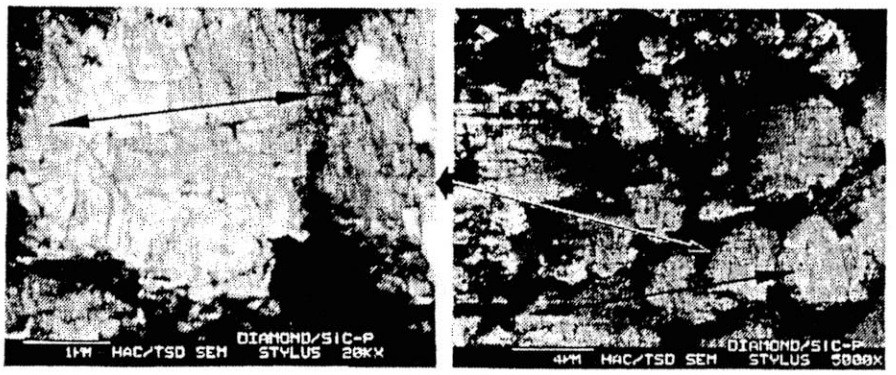

Figure 13. Tensile cracks on worn cauliflower tips of "sp^3"-coated α-SiC pin rubbed against "sp^3" film; double-headed arrows indicate direction of oscillatory sliding.

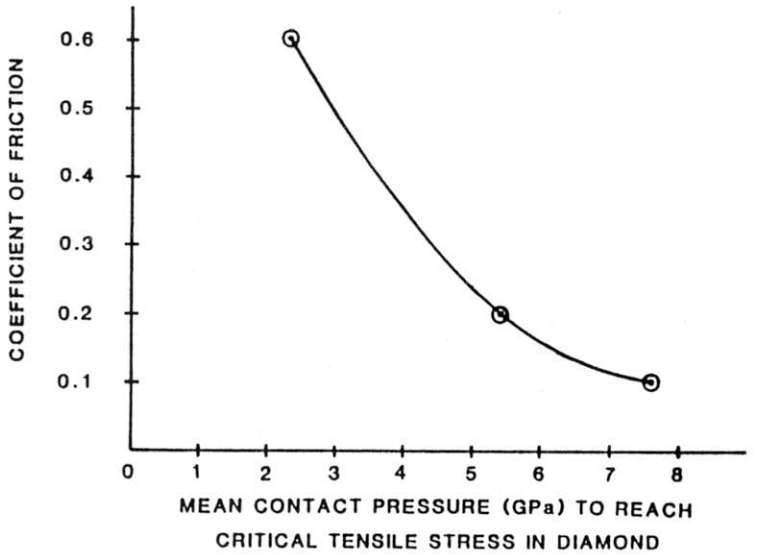

Figure 14. Sliding-induced tensile cracking on diamond as a function of friction coefficient; after (41).